Monthly Notices of the ROYAL ASTRONOMICAL SOCIETY

MNRAS **532,** 3682–3693 (2024) https://doi.org/10.1093/mnras/stae1669
Advance Access publication 2024 July 09

The Physalis system: discovery of ORC-like radio shells around a massive pair of interacting early-type galaxies with offset X-ray emission

Bärbel S. Koribalski [1,2]★ Ildar Khabibullin [3,4,5] Klaus Dolag,[3,4] Eugene Churazov [4,5] Ray P. Norris [1,2] Ettore Carretti [6] Andrew M. Hopkins,[7] Tessa Vernstrom [8,9] Stanislav S. Shabala [10] and Nikhel Gupta[9]

[1]*Australia Telescope National Facility, CSIRO Astronomy and Space Science, PO Box 76, Epping, NSW 1710, Australia*
[2]*School of Science, Western Sydney University, Locked Bag 1797, Penrith, NSW 2751, Australia*
[3]*Universitäts-Sternwarte, Fakultät für Physik, Ludwig-Maximilians-Universität München, Scheinerstr 1, D-81679 München, Germany*
[4]*Max-Planck-Institut für Astrophysik, Karl-Schwarzschildstr 1, D-85748 Garching, Germany*
[5]*Space Research Institute (IKI), Profsoyuznaya 84/32, Moscow 117997, Russia*
[6]*INAF – Istituto di Radioastronomia, Via Gobetti 101, I-40129 Bologna, Italy*
[7]*School of Mathematical and Physical Sciences, Macquarie University, 12 Wally's Walk, North Ryde, NSW 2109, Australia*
[8]*International Centre for Radio Astronomy Research, The University of Western Australia, 35 Stirling Highway, Crawley, WA 6009, Australia*
[9]*CSIRO Space & Astronomy, PO Box 1130, Bentley, WA 6102, Australia*
[10]*School of Natural Sciences, University of Tasmania, Private Bag 37, Hobart, TAS 7001, Australia*

Accepted 2024 July 5. Received 2024 July 4; in original form 2024 April 15

ABSTRACT

We present the discovery of large radio shells around a massive pair of interacting galaxies and extended diffuse X-ray emission within the shells. The radio data were obtained with the Australian Square Kilometre Array Pathfinder (ASKAP) in two frequency bands centred at 944 MHz and 1.4 GHz, respectively, while the X-ray data are from the *XMM–Newton* observatory. The host galaxy pair, which consists of the early-type galaxies ESO 184-G042 and LEDA 418116, is part of a loose group at a distance of only 75 Mpc (redshift $z = 0.017$). The observed outer radio shells (diameter ∼145 kpc) and ridge-like central emission of the system, ASKAP J1914−5433 (Physalis), are likely associated with merger shocks during the formation of the central galaxy (ESO 184-G042) and resemble the new class of odd radio circles (ORCs). This is supported by the brightest X-ray emission found offset from the centre of the Physalis system, instead centred at the less massive galaxy, LEDA 418116. The host galaxy pair is embedded in an irregular envelope of diffuse light, highlighting ongoing interactions. We complement our combined radio and X-ray study with high-resolution simulations of the circumgalactic medium (CGM) around galaxy mergers from the *Magneticum* project to analyse the evolutionary state of the Physalis system. We argue that ORCs/radio shells could be produced by a combination of energy release from the central active galactic nucleus and subsequent lightening up in radio emission by merger shocks travelling through the CGM of these systems.

Key words: galaxies: evolution – galaxies: groups: general – galaxies: individual: ESO 184-G042 – galaxies: interactions – radio continuum: galaxies – X-rays: galaxies.

1 INTRODUCTION

The Evolutionary Map of the Universe (EMU; Norris et al. 2011, 2021b) and the Widefield ASKAP *L*-band Legacy All-sky Blind surveY (WALLABY; Koribalski 2012; Koribalski et al. 2020) sky surveys are the two largest science projects currently underway with the Australian Square Kilometre Array Pathfinder (ASKAP; Johnston et al. 2008; Hotan et al. 2021). While both surveys produce deep radio continuum images, WALLABY's main focus is on H I imaging of the nearby Universe. In addition to millions of radio continuum point sources, ASKAP surveys reveal low surface brightness (LSB) emission structures in many shapes and sizes, including cluster haloes and relics, giant radio galaxies with fading lobes, nearby star-forming disc galaxies, Galactic supernova remnants, and diffuse radio emission of yet unknown origin (see e.g. Koribalski 2022). With the EMU survey now ∼20 per cent complete, the source numbers in each category are rising, improving our knowledge of their properties, occurrence rates, and formation mechanisms.

Odd radio circles (ORCs; Koribalski et al. 2021; Norris et al. 2021a) and similar radio rings/shells around massive early-type galaxies (see Section 1.1) are a recent addition to these extended LSB structures. Using high-resolution cosmological simulations, Dolag et al. (2023b) show that outward moving merger shocks resembling ORCs occur in the circumgalactic medium (CGM) of massive early-type galaxies at certain stages during their formation (see Section 1.2). Such merger shells have not previously been

★ E-mail: Baerbel.Koribalski@csiro.au

observed around galaxy pairs or groups, although such shock fronts are known, for example, in Stephan's Quintet ($z = 0.022$; Geng et al. 2012; Appleton et al. 2023, and references therein) and associated with the early-type galaxy pair NGC 7619/26 ($z = 0.013$) within the Pegasus group (Randall et al. 2009).

On larger scales ($\gtrsim$1 Mpc), merger-driven shocks are well known in galaxy clusters where they often result in arc-shaped single or double radio relics (e.g. van Weeren et al. 2019) and provide key information on the merger dynamics and evolutionary state of the cluster. Symmetric double relics are typically found in face-on cluster mergers, where they form partial shells/circles (in projection) with diameters of 2–3 Mpc (e.g. Koribalski et al. 2024, and references therein). In the early phase of a major merger, shocks may form in the compression zone between two fast-approaching clusters (see e.g. Gu et al. 2019) and X-ray emission is typically detected around the cluster centre, between the relics. Merger shocks propagating down a steep density gradient can maintain their strength and remain efficient accelerators of particles even at large distances from the cluster centre (e.g. Zhang et al. 2019).

Here we present the Physalis[1] system (ASKAP J1914−5433, see Fig. 1), named after its multishell radio morphology. It is the closest currently known ORC-like system associated with a galaxy pair. The primary host is the S0 galaxy ESO 184-G042 ($z = 0.017$), and its companion is LEDA 418116; see Table 1 for a summary of the Physalis system properties. In Section 1.1, we briefly describe the small sample of published ORCs (and ORC candidates) around massive early-type galaxies and summarize proposed formation scenarios. We then highlight the simulations by Dolag et al. (2023b) that suggest ORCs are formed by outward moving merger shocks (see Section 1.2). In Section 2, we describe the ASKAP radio continuum and *XMM–Newton* X-ray observations and data processing, followed by our results in Section 3. We discuss our findings in Section 4, and present our conclusions in Section 5.

1.1 Odd radio circles

ORCs are a newly discovered class of astronomical sources (Koribalski et al. 2021; Norris et al. 2021a), showing edge-brightened rings or shells of radio emission with diameters of ∼300–500 kpc, but no detected counterparts at non-radio wavelengths. Here, we focus on those ORCs where energetic events during the evolution of their central early-type host galaxies are likely responsible for their origins. As such galaxies contain supermassive black holes (SMBHs), their jet emission, feeding habits, etc. may play a role (e.g. Velović et al. 2023). A number of formation scenarios have been proposed in the above papers, e.g. end-on radio lobes, giant blast waves, and starburst winds. A new idea, able to explain the formation of ORCs, was proposed by Dolag et al. (2023b) who found shock structures of similar shapes and sizes around massive early-type galaxies in their simulations (see Section 1.2). Other formation scenarios include radio remnants of precessing jets seen end-on (Nolting, Ball & Nguyen 2023), virial shocks (Yamasaki, Sarkar & Li 2024), active galactic nucleus (AGN) jet-inflated bubbles (Lin & Yang 2024), and re-energized vortex rings (phoenixes; Shabala et al. 2024).

The first three single ORCs – ORC 1 (Norris et al. 2021a, 2022), ORC 4 (Norris et al. 2021a), and ORC 5 (Koribalski et al. 2021) – are centred on massive early-type galaxies at redshifts $z = 0.55$, 0.45, and 0.27, respectively. Using long-slit spectra, Rupke et al. (2024) recently confirm these redshifts and find that all three host galaxies have high stellar velocity dispersions ($\gtrsim$230 km s^{-1}), old (>1 Gyr) stellar populations, and LINER (low-ionization nuclear emission-line region)-type spectra. Furthermore, [O III] imaging by Coil et al. (2024) reveals an extended (40 kpc) ionized disc around the host galaxy of ORC 4.

Other ORCs and ORC-like sources include SAURON (Spectroscopic Areal Unit for Research on Optical Nebulae), a complex, ring-like radio structure with a luminous red galaxy ($z \approx 0.55$) at its centre (Lochner et al. 2023), and ORC J1027−4422, a partial ring with an extended central radio source (Koribalski et al. 2024), as well as J0849−0457 ($z \approx 0.34$, size = 70 kpc) and J2223−4834 ($z \approx 0.27$, size = 370 kpc) found in ASKAP survey images by Gupta et al. (2022), which appear to be associated with interacting galaxies in groups. Peculiar envelopes of diffuse radio emission around early-type galaxies were also recently highlighted by Kumari & Pal (2024a, b): J1507+3013 ($z = 0.08$, size = 68 kpc) has an ORC-like morphology and J1407+0453 ($z = 0.13$, size = 160 kpc) includes a horseshoe-shaped ring and is associated with an early-type galaxy group.

A few much closer systems with radio shells, which allow for the detection of hot gas via X-ray emission (Kraft et al. 2022; Dolag et al. 2023a), include the double-shell system ORC 6 ($z = 0.125$), the Cloverleaf system ($z = 0.046$; Bulbul et al. 2024; Koribalski et al., in preparation) – both mentioned in Dolag et al. (2023b) – and the Physalis system ($z = 0.017$) described here. The resolved radio structures discovered by ASKAP in the intragroup medium of these systems are shedding new light on the formation and evolutionary processes of their central host galaxies. Follow-up, high-resolution observations at a wide range of frequencies are essential to distinguish between different models.

For completeness, we mention ORC 2 (ring size ∼80 arcsec or 380 kpc) and its neighbour ORC 3 (a diffuse emission patch), discovered in ASKAP images by Norris et al. (2021a), which are different from the single ORCs with massive central galaxies. The pair are likely the lobes of a restarted and bent radio galaxy at redshift $z \approx 0.33$ (Macgregor et al., in preparation). For a possible formation scenario see Shabala et al. (2024). Much smaller ring-like structures are known within some radio lobes such as the Teacup (Lansbury et al. 2018), 3C 310 (Kraft et al. 2012), and the 'doughnut' in NGC 6109 (Rawes, Birkinshaw & Worrall 2018) with sizes of 10, 40, and 6 kpc, respectively, likely formed by a fast precessing jet.

1.2 Galaxy merger shocks in simulations

Using high-resolution cosmological simulations, Dolag et al. (2023b) find outward-moving merger shocks resembling ORCs in the CGM of massive early-type galaxies, residing around the virial radius. In their simulations, shock-accelerated electrons produce synchrotron emission within magnetic fields penetrating the CGM. The origin of such shocks is mergers during the formation of the central elliptical galaxy. The prediction from the simulations is that radio-detectable, outward moving shocks/merger shells should sometimes be observable around massive early-type galaxies during their formation. Such merger shells are rare, both observationally and in the cosmological simulations. Interestingly, the simulations show hot gas residing within the shells, similar to hot haloes in cluster centres bounded by radio relics. Finding radio rings/shells around nearby galaxies, such as the Physalis system presented here, allows for much more detailed multiwavelength studies than have been possible so far.

[1]Physalis is a small orange fruit surrounded by papery shells.

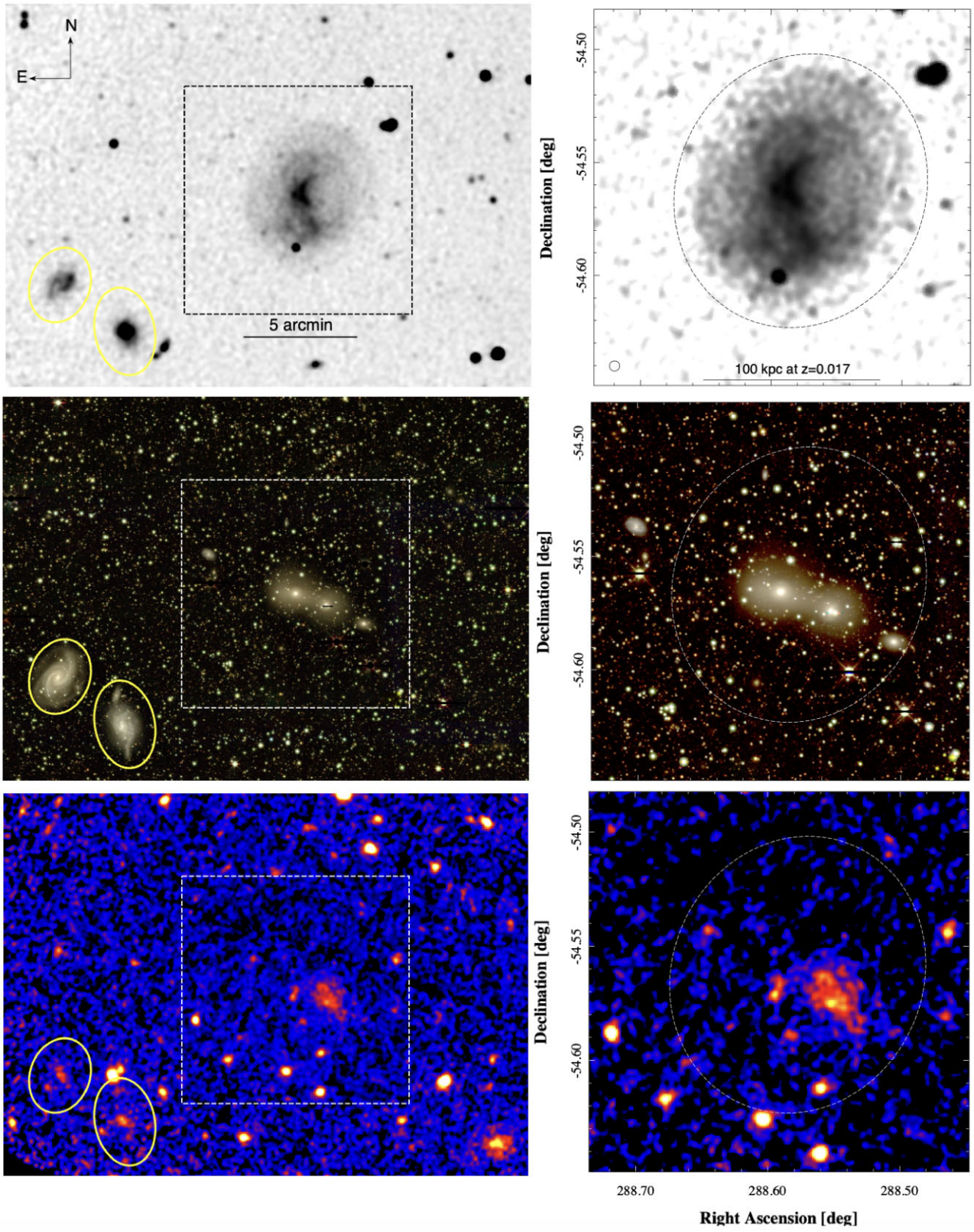

Figure 1. Left: The Physalis system (ASKAP J1914−5433, $z = 0.017$) and the foreground spiral galaxy pair IC 4837/9 (two small ellipses). Right: Zoom-in of the Physalis system. Its radio extent is marked by an ellipse of size 7.4 arcmin × 6.6 arcmin (PA = 156°). Top: ASKAP EMU 944 MHz radio continuum image. The ASKAP synthesized beam (15 arcsec) is displayed in the bottom left corner. Middle: Dark Energy Spectroscopic Instrument (DESI) Legacy Survey Data Release 10 (DR10) *gri*-band optical image (Dey et al. 2019). Bottom: *XMM–Newton* 0.5–2.5 keV X-ray surface brightness image (resolution ∼15 arcsec).

Table 1. Properties of the Physalis system.

	Physalis system		Refs
Name	ASKAP J1914−5433		
Host galaxy pair	ESO 184-G042	LEDA 418116	
Optical morph. type	S0 pec	SAB0: pec	RC3
Systemic velocity	5135 km s^{-1}	5252 km s^{-1}	W03, D12
Distance	75 Mpc		
Velocity dispersion	176 ± 21 km s^{-1}	–	W03
Diameter (B_{25})	80 arcsec × 56 arcsec	77 arcsec × 44 arcsec	L89, M14
Diameter (B_{26})	136 arcsec × 94 arcsec	–	L89
Diameter (B_{27})	197 arcsec × 136 arcsec	–	L89
Position angle (B_{26})	78°	–	L89
B-band magnitude	14.0	14.7	L89, M14
K-band magnitude	10.0	10.8	S06
Log stellar mass ($M_\odot$)	11.1	10.7	

Note. References: RC3 (de Vaucouleurs et al. 1991), W03 (Wegner et al. 2003), D12 (Díaz-Giménez et al. 2012), L89 (Lauberts & Valentijn 1989), M14 (Makarov et al. 2014), and S06 (Skrutskie et al. 2006).

Table 2. ASKAP radio continuum observations and image properties. SB stands for scheduling block.

ASKAP SB	51574	51537
Date	2023 July 24	2023 July 22
Integration time (h)	10	8
Field of view (deg^2)	∼30	∼30
Centre freq (MHz)	943.5	1367.5
Bandwidth (MHz)	288	144
rms (μJy beam^{-1})	∼40	∼30
Resolution (arcsec)	15	8.7 × 8.0

2 OBSERVATIONS AND DATA ANALYSIS

2.1 ASKAP

Fully processed radio continuum images from the ASKAP were obtained through the CSIRO ASKAP Data Science Archive (CASDA).[2] For a description of the telescope, data processing, and science highlights, see Johnston et al. (2008), Hotan et al. (2021), and Koribalski (2022). We primarily use the ASKAP 944 MHz images at 15 arcsec resolution as they provide the best signal-to-noise ratio. ASKAP 1.4 GHz radio continuum images at ∼10 arcsec resolution are also available. A summary of the observational and image properties is given in Table 2.

2.2 *XMM–Newton*

We obtained a 21 ks long integration of the Physalis system with the X-ray space observatory *XMM–Newton* (Jansen et al. 2001) using the European Photon Imaging Camera (EPIC) in the 0.5–2.5 keV energy range. The observations were carried out on 2023 September 15 during Directors Discretionary Time (DDT) under Project ID 0932390101 (PI: Norbert Schartel). The data were retrieved from the *XMM–Newton* archive, reduced using the standard pipeline and processed via the Science Analysis System,[3] as well as custom data analysis software extensively used previously for *XMM–Newton* data analysis of extended X-ray sources (Churazov et al. 2003). The observation was characterized by a stable particle background without significant flares, resulting in filtering out of only 1 per cent for the MOS and 10 per cent of the EPIC-pn data. Our X-ray surface brightness images are background subtracted as well as exposure- and vignetting corrected (see Fig. 1). We show the combined signal from the EPIC-pn and MOS1 + MOS2 detectors. The X-ray image resolution is ∼15 arcsec within the central ∼10 arcmin of the field. For the spectral analysis, we consider only the combined EPIC MOS data extracted from the region of the brightest emission, leaving further investigation of fainter diffuse emission for future exploration involving upcoming an order of magnitude deeper data (Khabibullin et al., in preparation).

[2] https://data.csiro.au/domain/casdaObservation
[3] https://www.cosmos.esa.int/web/xmm-newton/sas-threads

3 RESULTS

To set the scene we first introduce the Physalis host galaxy system, then present our radio continuum results, followed by our X-ray results.

3.1 The host galaxy system

ESO 184-G042 is the brightest member of a loose galaxy group (Díaz-Giménez et al. 2012; Tempel et al. 2018), which consists of three early-type galaxies and a small spiral galaxy that are linearly aligned (see Fig. 1 and Table 1). The closest neighbour of ESO 184-G042 is the galaxy LEDA 418116, located 1.4 arcmin or 30 kpc to the west. The extended envelope of diffuse stellar light around these two brightest group galaxies is remarkable, spanning at least 3.5 arcmin (∼76 kpc, see Fig. 2). The large amount of intragroup light is indicative of strong tidal interactions (e.g. Spavone et al. 2018; Montes 2022). The third member of the early-type triplet is the galaxy LEDA 417985 ($v_{\rm sys}$ = 5550 km s^{-1}; Jones et al. 2009), located further west, at a projected distance of 3.3 arcmin or 72 kpc from ESO 184-G042. The stellar masses of ESO 184-G042, LEDA 418116, and LEDA 417985 are 1.1, 0.6, and 0.2 × 10^{11} $M_\odot$ as obtained from their *K*-band magnitudes (see Table 1). We note that Wen & Han (2024) derive stellar masses of 10^{11} $M_\odot$ for ESO 184-G042 and 10^{10} $M_\odot$ for LEDA 417985 based on Dark Energy Survey (DES) Data Release 10 (DR10) and *Wide-field Infrared Survey Explorer* colours; no estimate is given for LEDA 418116 in their catalogue, which is partially obscured by a Galactic foreground star. The values are within the typical 20 per cent uncertainties of stellar mass estimates. Estimates of the R_{500} radius and M_{500} mass for the host galaxy pair are given in Table 3. The fourth group member is the spiral galaxy LEDA 418483 ($v_{\rm sys}$ = 5143 km s^{-1}; Jones et al. 2009), located 4.2 arcmin or 92 kpc east of ESO 184-G042. The projected linear extent of the group is 164 kpc. Interestingly, a statistical study by Rong, Shen & Hua (2024) finds alignment between loose galaxy triplets and their host filaments. The relative line-of-sight velocity of the host galaxy pair is quite small (117 ± 52 km s^{-1}, see Table 1), implying that the merger might be happening in the plane of the sky, as also suggested by the galaxy alignment and the morphology of the radio emission. While we detect a large envelope of diffuse intragroup light around the pair, no other signatures of tidal interactions are seen (e.g. tidal tails, shells, and umbrella features). Stellar shells around elliptical galaxies have been known for a long time (Malin & Carter 1980, 1983), and they typically form in dry (gas-poor) radial mergers (Karademir et al. 2019), while the formation of ORCs requires wet (gas-rich) and not very radial mergers (see Section 4.2). The line-of-sight velocity dispersion of the galaxies associated with the group is

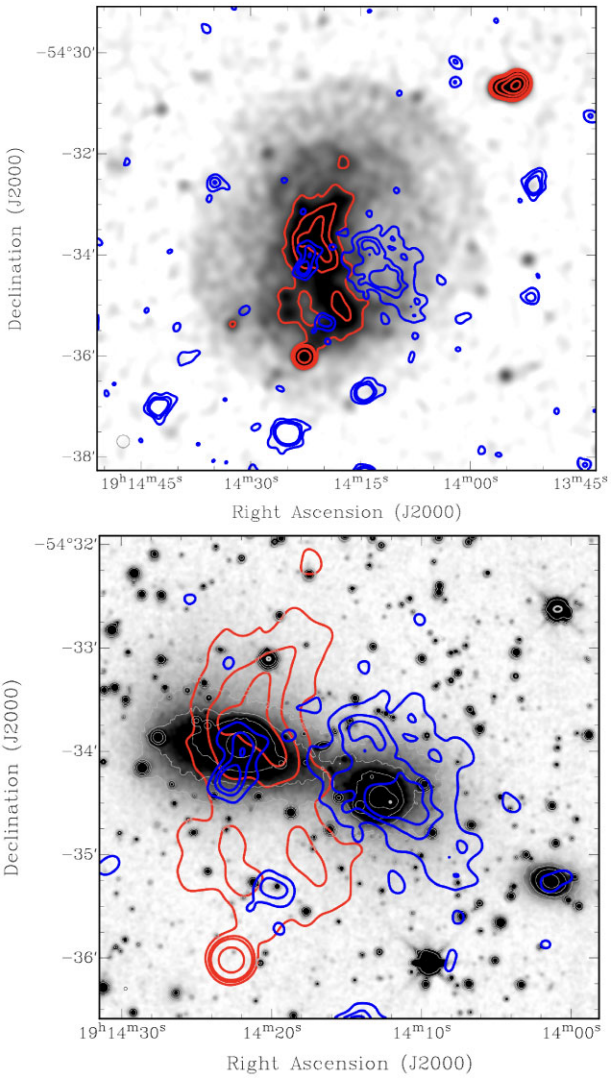

Figure 2. Top: Radio continuum image of the Physalis system (ASKAP J1914−5433) made by combining the ASKAP 944 MHz and 1.4 GHz images overlaid with (a) ASKAP radio continuum emission (red contours at 1, 1.5, 2, 5, 10, and 20 mJy beam^{-1}) and (b) *XMM–Newton* X-ray emission (blue contours at 0.0002, 0.0003, and 0.0004 counts s^{-1} cm^{-2} arcmin^{-2}). The ASKAP synthesized beam (15 arcsec) is displayed in the bottom left corner. Bottom: DESI DR10 g-band optical image (smoothed with a 2 arcsec Gaussian) of the Physalis host galaxy pair, ESO 184-G042 and LEDA 418116, overlaid with the same contours as above. Here we highlight the offset between the bright radio ridge, centred on ESO 184-G042, and the brightest X-ray emission centred on the neighbour, LEDA 418116.

$\sim$180 km s^{-1}, which provides a dynamical mass estimate of $M_{200c} \approx 8 \times 10^{12}$ M$_\odot$ (e.g. Evrard et al. 2008; Ferragamo et al. 2021) and $M_{500} \approx 5.8 \times 10^{12}$ M$_\odot$ (see Table 2). This estimate is likely an underestimate, given the likely merging geometry close to the plane of the sky.

3.2 Radio continuum

Fig. 1 shows the ASKAP EMU 944 MHz radio continuum image of the Physalis system and the foreground galaxy pair IC 4837/9 as well as a close-up of Physalis. The latter highlights the faint outer radio shells and bright central ridge. The radio ridge is elongated in the direction perpendicular to the axis connecting the four group galaxies. Both, shells and ridge, are centred on the massive early-type galaxy ESO 184-G042 (see Fig. 2). Some diffuse radio emission is also detected between the shells and the ridge. The overall size of the Physalis system is $\sim$400 arcsec $\times$ 320 arcsec (PA $\approx 156^\circ$) or 145 kpc $\times$ 116 kpc. That is less than half the diameter of the more distant single ORCs (Koribalski et al. 2021; Norris et al. 2021a). The velocity dispersion of ESO 184-G042 (176 km s^{-1}; Wegner et al. 2003) is close to that of the ORC host galaxies (Coil et al. 2024; Rupke et al. 2024). Fig. 3 highlights the distinct radio shells both in the observations (left) and in galaxy-merger simulations from the *Magneticum* project (right). Red colours show the excess observed radio emission; inner and outer shells are visible. The most prominent outer radio shell is in the north-west (NW), curving towards the south, then connecting to the fainter, eastern shell, forming nearly a full circle. Secondary radio shells are seen inside the NW shell, around the bright central ridge.

We measure total flux densities of $S_{944\,\mathrm{MHz}} = 145 \pm 2$ mJy and $S_{1.4\,\mathrm{GHz}} = 79 \pm 2$ mJy, resulting in a spectral index of $\alpha = -1.64 \pm 0.11$, where $S_\nu \propto \nu^\alpha$. For the above flux measurements a background radio source ($\sim$6 mJy), located south of the Physalis centre, was excluded. Some extended radio emission may have been filtered out, which implies that both flux estimates have lower limits. The quoted uncertainties are from our measurements; for an analysis of the ASKAP flux calibration uncertainties ($\leq$10 per cent), see Duchesne et al. (2024). For the brightest part of the central ridge, which is also detected in Sydney University Molonglo Sky Survey at 843 MHz (19.1 $\pm$ 2.4 mJy; Mauch et al. 2003), we measure flux densities of $S_{944\,\mathrm{MHz}} = 15.7$ mJy and $S_{1.4\,\mathrm{GHz}} = 8.8$ mJy, resulting in $\alpha \approx -1.6$. This suggests that the outer radio shells are similarly steep. The Physalis radio shells contain about 60 per cent of the total flux. Deeper interferometric images at a wide range of frequencies are needed to study the spectral index variations in the inner ridge and outer shells of Physalis.

The Physalis system is also detected at low frequencies (from 72 to 231 MHz) in the GaLactic and Extragalactic All-sky Murchison Widefield Array (GLEAM) survey (Hurley-Walker et al. 2017, 2022), where it is catalogued as GLEAM J191420−543356 with a spectral index of $\alpha = -1.0 \pm 0.1$. Based on the catalogued source diameters, the source is extended in all GLEAM bands. For example, the catalogued flux density and source diameter in the GLEAM 171–230 MHz band are 545 $\pm$ 36 mJy and 242 arcsec $\times$ 183 arcsec (PA = 157°), respectively. The angular resolution at 200 MHz is $\sim$2 arcmin. Based on the catalogued GLEAM spectral index, we would expect ASKAP flux densities of 116 $\pm$ 28 mJy at 944 MHz and 80 $\pm$ 20 mJy at 1.4 GHz for Physalis, which agrees within the uncertainties with the measured ASKAP fluxes given above.

3.3 X-ray emission

Our *XMM–Newton* DDT observations of the Physalis system resulted in a clear detection of diffuse X-ray emission within the radio shells. We find the hot gas to be cospatial with the less massive galaxy (LEDA 418116) in the merging host pair and anticorrelating with the surface brightness of the radio emission (see Fig. 2). Our 21 ks long integration already allowed for the collection of $\sim$1000 EPIC counts from the Physalis system, enabling not only the detection of extended X-ray emission but also the characterization of its hot gas content and temperature. We do not detect signatures of currently X-ray bright AGN in the host galaxy pair.

Table 3. Properties of ORCs and radio shell systems as well as their host galaxies. The columns are: (1)–(2) source names, (3) redshift z, (4) ORC diameter, (5) D_{500} derived from M_{500}, (6) the measured 150 MHz flux density S_{150}, (7) the derived 150 MHz radio power P_{150}, (8) the stellar mass $M_\star$ of the central galaxies from Zou et al. (2019) for ORC 1, 4, 5 and derived from their K-band luminosity for ORC J1027−4422, Cloverleaf, and Physalis. For Physalis, we give the combined mass of the host galaxy pair. (9) The M_{500} estimates are based on the stellar-to-halo mass ($M_\star \propto M_{200c}$) relation from Girelli et al. (2020), where the range only reflects the uncertainty of the averaged value and does not include the scatter of individual systems. For the radio shell systems, M_{500} estimates are also inferred from the X-ray temperature and luminosity (in bold font) using the scaling relations from Lovisari et al. (2021); the X-ray values for the Cloverleaf system are from Bulbul et al. (2024). The last value (also in bold font) is based on the virial mass derived from velocity data. Conversion between virial mass, M_{200c}, and M_{500} are made based on the fitting formulae given in Ragagnin et al. (2021). The last column gives the references.

Source name		z	Size (kpc)	S_{150} (mJy)	P_{150} (10^{24} W Hz^{-1})	$M_\star$ (10^{11} M$_\odot$)	M_{500} (10^{12} M$_\odot$)	R_{500} (kpc)	Refs
(1)	(2)	(3)	(4)	(5)	(6)	(7)	(8)	(9)	(10)
ORC J2103−6200	ORC 1	0.55	520	38 ± 6	46 ± 7	5.0 ± 0.5	260–380	513	1, 2
ORC J1555+2726	ORC 4	0.45	520	28 ± 3	21 ± 2	1.8 ± 0.2	16–25	234	1
ORC J0102−2450	ORC 5	0.27	300	17 ± 1	3.9 ± 0.2	1.0 ± 0.2	2.4–3.4	186	3
ORC J1027−4422		∼0.3	400	<7.5	<5	0.3	0.51–0.52	120	4
ASKAP J1137−0050	Cloverleaf	0.046	400	∼2600	13.0 ± 0.5	1.4	7.1–10, **20**, **6**, **9**	323	5
ASKAP J1914−5433	Physalis	0.017	145	545 ± 4	0.37 ± 0.01	1.7	15–20, **12**, **14**, **6**	326	This paper

Note. References: 1 – Norris et al. (2021a), 2 – Norris et al. (2022), 3 – Koribalski et al. (2021), 4 – Koribalski et al. (2024), and 5 – Koribalski et al. (in preparation).

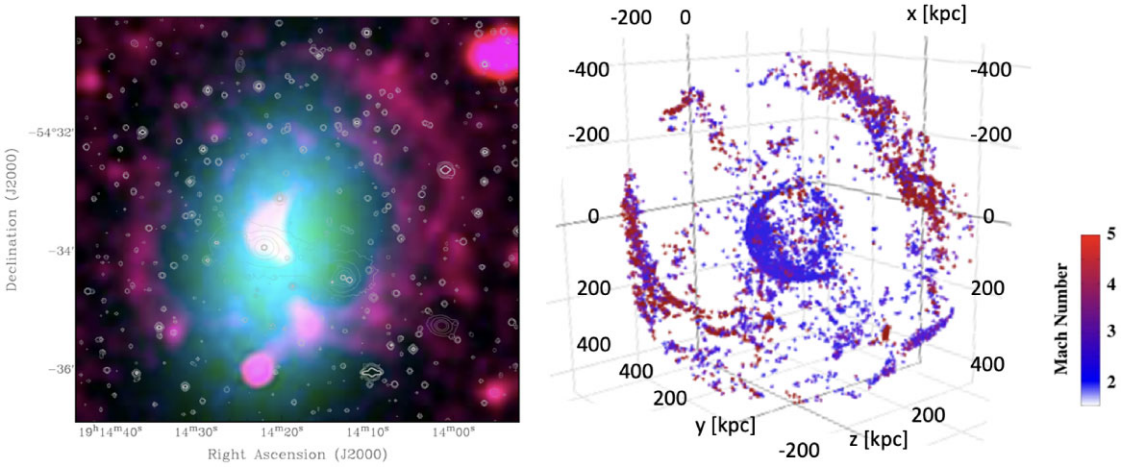

Figure 3. Left: The Physalis system (ASKAP J1914−5433). To emphasize the outer radio shells, we show the ASKAP 944 MHz radio continuum image (blue), a Gaussian model (green), and the residual radio emission (red) overlaid with grey contours from the optical DES DR10 g-band image. Right: Snapshot of a galaxy merger simulation producing large-scale relics like those seen in the left panel. Inner and outer merger structures are visible at a range of Mach numbers. Interactive 3D visualizations of the galaxy merger shocks are available at http://www.magneticum.org/complements.html#Compass presented in Dolag et al. (2023b).

Fig. 4 shows a composite image of the X-ray and radio continuum emission (left) as well as the extracted X-ray spectrum and best-fitting emission model (right) obtained by fitting the X-ray spectrum with a thermal emission model of hot optically thin plasma. The latter is computed using XSPEC (Arnaud 1996) and an APEC (Astrophysical Plasma Emission Code; Smith et al. 2001) model with a metallicity of $0.2\,Z_\odot$. Assuming the line-of-sight extent of the region is comparable to its picture plane size, we estimate the electron number density of the hot X-ray gas at the level of $n_e \sim 10^{-3}$ cm^{-3}, so the thermal pressure is $P_{th} \approx 2 n_e \kappa T_e \sim 3 \times 10^{-12}$ erg cm^{-3}. The striking anticorrelation between radio and X-ray surface brightness suggests there might be a pressure balance between X-ray and radio-bright regions. In such a case, the total energy in the shell region would be $E_{tot} \sim 2 \times 10^{59}$ erg, with the dense X-ray gas contributing only a few per cent. The cooling time for the X-ray gas is $t_{cool} \sim 4 \times 10^8$ yr, providing us with an estimate for an upper limit of the age of the observed phenomenon.

3.4 The foreground spiral galaxy pair

The interacting galaxy pair IC 4837/39 lies ∼10 arcmin south-east of ESO 184-G042 (see Fig. 1). Both galaxies are detected in the ASKAP radio and *XMM–Newton* X-ray images. The galaxy pair is also detected in the H I Parkes All Sky Survey (HIPASS) – catalogued as HIPASS J1915−54b – with a flux density of 20.1 ± 4.0 Jy km s^{-1} and a systemic velocity of 2717 km s^{-1} (Koribalski et al. 2004). We measure the following ASKAP flux densities: IC 4837 (20 mJy at 1.4 GHz, 27 mJy at 944 MHz) and IC 4839 (11 mJy at 1.4 GHz, 15 mJy at 944 MHz); the flux uncertainties are ∼1 mJy. Both galaxies were observed as prime candidates for the host of LIGO (Laser Interferometer Gravitational-Wave Observatory) triggers G274296 ($z_{GW} > 0.42$; Ridley et al. 2024) and G284239 but no interesting transient candidates within the posterior constraints were identified (e.g. Yang et al. 2019).

The interacting galaxies associated with the Physalis radio shell system (D = 75 Mpc, see Fig. 2), while not previously considered

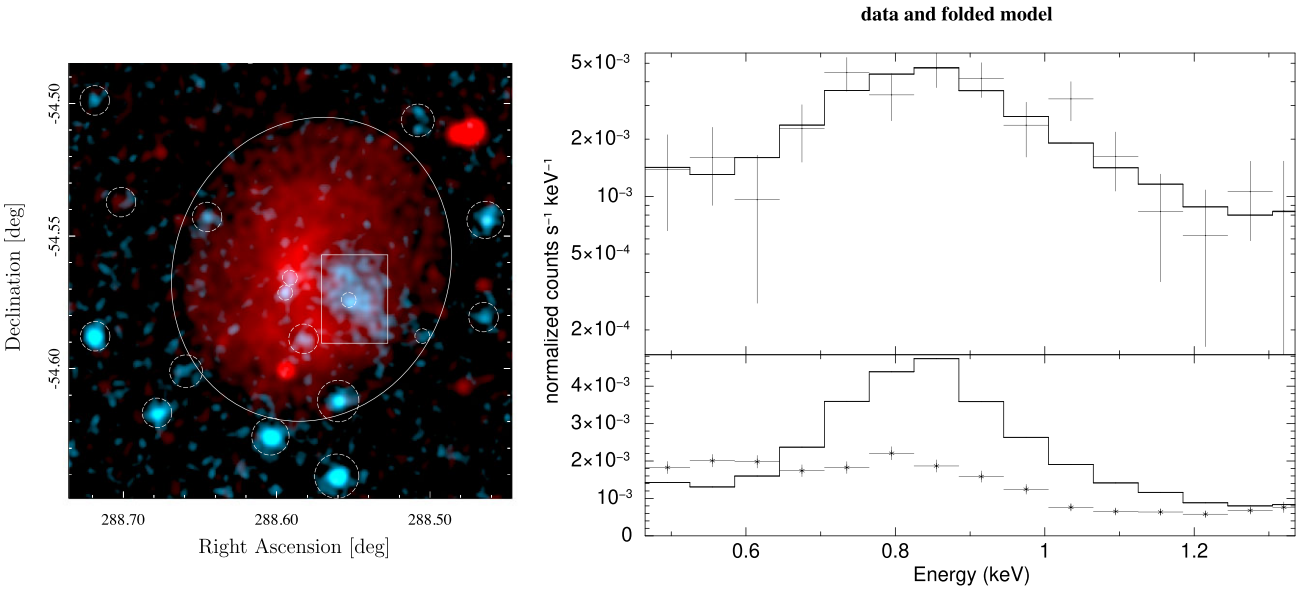

Figure 4. Composite image of the Physalis system (left) consisting of ASKAP radio continuum emission in red and 0.5–2.5 keV X-ray emission in cyan. The large ellipse highlights the extent of the radio emission (see also Fig. 1), while the small rectangle marks the extraction region for the X-ray spectrum. Background AGN, Galactic foreground stars, and X-ray emission associated with the three early-type galaxies in the Physalis system (see Fig. 2, bottom) are marked with small circles and were masked in the spectrum extraction procedure. The top right panel shows the X-ray spectrum from the rectangular region after subtracting the background estimate from the region confined by the ellipse, overlaid with the best-fitting thermal APEC model. The bottom right panel shows a comparison of this model with the background estimate, highlighting the energy range where the X-ray signal dominates over the background.

as possible hosts for these gravitational wave (GW) bursts, make interesting candidates. Dynamically formed stellar black hole (BH) binaries in globular clusters (GCs) are likely one of the main sources of GWs (Antonini & Gieles 2020; Antonini et al. 2023). The more massive a galaxy, the more GCs it contains (Forbes 2017), increasing the likelihood of GW events from the host galaxies of the Physalis system. Furthermore, mergers of stellar-mass BHs may be enhanced around SMBHs (Abbott et al. 2020).

4 DISCUSSION

In the following we discuss the merger-driven scenario, explore a counterpart found in *Magneticum*, and compare Physalis and similar radio shell systems to cluster relics.

4.1 The merger-driven scenario

The early-type galaxy ESO 184-G042 is the brightest and most massive member of a loose group of galaxies. Its nearest neighbour, LEDA 418116, is the second brightest galaxy of the group. The distribution of the optical light in the system (see Figs 1 and 2) reveals an elongation of their stellar bodies as well as surrounding diffuse intragroup light, indicating ongoing interactions heading towards the more violent final stage of the group's stellar core build-up. The line-of-sight velocity difference of these two galaxies is rather small, 117 ± 52 km s^{-1}, somewhat less than the central velocity dispersion of ESO 184-G042 ($\sigma = 176 \pm 21$ km s^{-1}; see Table 1) implying that either the merger proceeds in the plane of the sky or the system is currently at the apocentric phase when the line-of-sight separation between the galaxies is maximal. The former possibility is supported by the remarkable alignment of the central pair of galaxies with two other group members (LEDA 417985 and LEDA 418483), located at projected distances 70 and 90 kpc with the line-of-sight velocity offset around 400 and $\pm$50 km s^{-1}, respectively. Photometric and kinematic properties indicate that the group's total mass (dominated by dark matter) is at the level of $\sim 10^{13}$ M$_\odot$, meaning that the observed diffuse radio emission is concentrated in the innermost 20 per cent of the group's ~400 kpc virial radius (see also Table 3). A similar linear galaxy alignment is found for the galaxies associated with the Cloverleaf system that also exhibits ORC-like radio shells (Koribalski et al., in preparation). For a comparison of its properties with those of the Physalis system see Table 3.

The gravitational potential well of such groups is expected to be filled with diffuse X-ray emitting gas having temperatures of ~0.5 keV. The *XMM–Newton* X-ray image of the Physalis system reveals extended emission, ~40 kpc in diameter, concentrated well within the boundaries of the radio shells. Moreover, it appears to be cospatial with the second brightest galaxy in the group. The measured temperature of X-ray emitting gas $\kappa T_{\rm X} \approx 0.7$ keV is much higher than $kT \sim 0.2$ keV expected for an individual elliptical galaxy of that mass. The hot gas might be a shocked remnant of the core of the second brightest group galaxy (LEDA 418116), which stands out from the more diffuse gas of the system, which is harder to detect (e.g. similar to the case of the Bullet Cluster in Markevitch et al. 2002). It could also be the already formed core of the post-merger group, while the apparent cospatiality with the second brightest galaxy is a transient phenomenon resulting from the merger-induced displacement of the gas with respect to the total gravitational potential of the system (shaped by the distribution of merging dark matter substructures within it). Numerical simulations of the cosmological structure formation predict that such an occurrence can indeed take place, especially when gas-rich substructures are infalling into a diffuse atmosphere of a large system or if the merger proceeds in a 'catch-up' configuration, which allows for avoiding violent

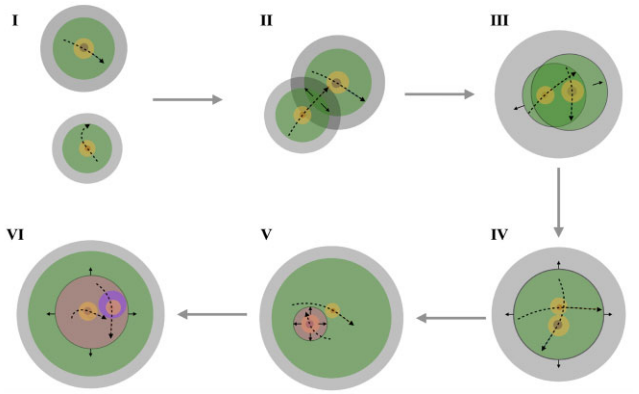

Figure 5. Schematic description of the proposed formation scenario for Physalis ORC shown as a sequence of snapshots, I → VI, separated by 400 Myr in time. The grey areas depict dark matter haloes of the two merging groups (radius $\sim R_{200c}$, i.e. the virial radius), green area – the region where most of the hot gas content of groups – is concentrated within $R \sim R_{500}$, the yellow regions show stellar bodies of the main group galaxies with the central regions containing respective SMBHs. The last two stages also contain a bubble of overheated material (shown in magenta) that was produced in an episode of powerful energy injection from the central part of one of the main galaxies, triggered by the merger-induced gas inflow into it. The last snapshot shows the shocked X-ray emitting gas (in violet) that managed to survive the passage of the bubble around it. The dashed arrows indicate the trajectories of the main galaxies, while the solid arrows mark the direction of the shock waves launched into the system.

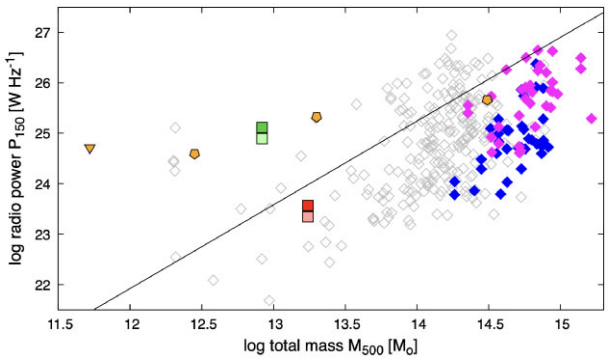

Figure 6. Scaling relation of 150 MHz radio power (P_{150}) versus total mass (M_{500}) for cluster radio relics (including candidates) from Jones et al. (2023, blue diamonds), including double relics from de Gasperin et al. (2014, pink diamonds), brightest cluster radio galaxies from Pasini et al. (2022, grey symbols), and our sample of ORCs and similar radio shell systems (see Table 3). ORCs are shown in orange, the Cloverleaf system in green, and the Physalis system in red. For the latter two, we show the system radio power (dark squares) as well as the approximate radio power of the shells alone (light squares; estimated to be around 60 per cent). The black line indicates $P_{150} \propto M_{500}^{5/3}$, which corresponds to self-similar scaling assuming the same fraction of merging energy going into the radio power (e.g. de Gasperin et al. 2014).

dispersion of the gas and causes more gentle sloshing motions instead. The schematic diagram in Fig. 5 shows six key steps in the proposed formation scenario for the Physalis system. In Fig. 6, we show the location of the Physalis system and other ORCs in the radio power versus mass diagram when compared to cluster relics and radio galaxies.

Upcoming, order-of-magnitude deeper *XMM–Newton* observations of the Physalis system will likely allow us to detect the full extent of the diffuse X-ray emission within the radio shells, which is only hinted at in the current DDT observations, allowing for a more detailed analysis (Khabibullin et al., in preparation).

As noted in Section 3.2, the Physalis system is also detected in GLEAM at frequencies from 72 to 231 MHz. This allows us to obtain an independent estimate of the total energy in relativistic particles and their ages. For the observed surface brightness at 200 MHz (545 ± 36 mJy) and the diameter of the Physalis system (∼150 kpc), minimum energy arguments (e.g. Beck & Krause 2005) yield $B \sim$ (1–3) μG, depending on the amount of energy associated with relativistic protons, and the energy density of the non-thermal (nt) component $\sim(0.6\text{–}4) \times 10^{-13}$ erg cm^{-3}. The larger value corresponds to a commonly used assumption that there are ∼100 times more relativistic protons than electrons with similar energies (Beck & Krause 2005), which we also adopt here. The corresponding pressure of this gas phase (1/3 of the energy density) $P_{\rm nt} \sim 1.5 \times 10^{-13}$ erg cm^{-3} is lower than the pressure of X-ray emitting gas $P_{\rm th} \sim 3 \times 10^{-12}$ erg cm^{-3}. This suggests that in order to be in pressure equilibrium, either a substantial departure from the minimum energy configuration is needed or there is an extra thermal (presumably hot and low-density) component cospatial with relativistic particles. The above arguments also provide a lower limit on the total non-thermal energy content within a sphere of radius $r = 80$ kpc: $E_{\rm nt} \sim 2 \times 10^{58}$ erg. Given that the Physalis system is detected at ∼1 GHz frequencies, the upper limit on the age of the latest episode of electrons' acceleration is set by their cooling time due to synchrotron and inverse Compton losses in a few μG field, $t_{\rm cool} \sim 10^8$ yr.

4.2 A counterpart in *Magneticum*

ORCs are rare phenomena, occurring with a frequency of around one per 0.05 Gpc^3 as estimated by Norris et al. (2022). This means that (1) very large simulation volumes are needed to identify counterparts, while having hosts that fall in the range of small groups, and (2) high resolution is needed to follow the evolution of this class of objects within such large volumes. One almost unique simulation that fulfils both these requirements is *Box2b/hr* from the *Magneticum* simulation set,[4] which follows a volume of $(640\,h^{-1}\,{\rm cMpc})^3$ with a total of 2×2880^3 particles, allowing the particles masses to be 6.9×10^8, 1.4×10^8, and $3.5 \times 10^7\,h^{-1}\,{\rm M}_\odot$, respectively, for dark matter, gas, and the stellar particles, where the latter have a gravitational softening of $\epsilon = 2\,h^{-1}$ ckpc ($h = H_0/(100$ km s^{-1} Mpc^{-1} is the Hubble constant). This results in a completeness limit for galaxies of roughly $10^{9.5}\,h^{-1}$ M$_\odot$. The simulations include the treatment of cooling through tables from Wiersma et al. (2009) as well as star formation and galactic winds with velocities of 350 km s^{-1} (Springel & Hernquist 2002). Metal species (namely, C, Ca, O, N, Ne, Mg, S, Si, and Fe) are tracers explicitly following in detail the chemical enrichment by Type Ia supernova, Type II supernova, and asymptotic giant branch (Tornatore et al. 2003, 2007) from the evolving stellar population. BHs and associated AGN feedback are treated following Springel, Di Matteo & Hernquist (2005), with various improvements (Fabjan et al. 2010; Hirschmann et al. 2014) for the detailed treatment of the BH sink particles and the different feedback modes. Isotropic thermal conduction of 1/20 of the standard *Spitzer* value (Dolag et al. 2004) is included. The numerical scheme follows an improved formulation of smoothed particle hydrodynamics (SPH) utilizing a low-viscosity scheme to track turbulence (Dolag et al. 2005; Beck

[4] http://www.magneticum.org/simulations.html

et al. 2016) and higher order SPH kernels (Dehnen & Aly 2012) for better sampling of the fluid.

The cosmology adopted for these simulations is the 7-year *Wilkinson Microwave Anisotropy Probe* from Komatsu et al. (2011), with a total matter density of $\Omega_{\rm m} = 0.272$, of which 16.8 per cent are baryons, the cosmological constant $\Lambda_0 = 0.728$, the Hubble constant $H_0 = 70.4$ km s^{-1} Mpc^{-1}, the index of the primordial power spectrum $n = 0.963$, and the overall normalization of the power spectrum $\sigma_8 = 0.809$. Haloes and galaxies are identified using SUBFIND (Springel et al. 2001; Dolag et al. 2009), where the centre of a halo is defined as the position of the particle with the minimum of the gravitational potential. The virial mass, $M_{\rm vir}$, is defined through the spherical overdensity as predicted by the generalized spherical top-hat collapse model (Eke, Cole & Frenk 1996) and, in particular, it is referred to $R_{\rm vir}$, whose overdensity to the critical density follows equation (6) of Bryan & Norman (1998).

Previous studies have demonstrated that the galaxy physics implemented in the *Magneticum* simulations leads to an overall successful reproduction of the basic galaxy properties, like the stellar mass function (Naab & Ostriker 2017; Lustig et al. 2023), the environmental impact on galaxy properties (Lotz et al. 2019), as well as the associated AGN population and their evolution (Hirschmann et al. 2014; Steinborn et al. 2016; Biffi, Dolag & Merloni 2018b). At cluster scales, the *Magneticum* simulations have demonstrated to reproduce the observable X-ray luminosity relation (Biffi, Dolag & Böhringer 2013), the pressure profile of the intracluster medium (ICM; Gupta et al. 2017) and the chemical composition (Dolag, Mevius & Remus 2017; Biffi, Mernier & Medvedev 2018a) of the ICM, the high concentration observed in fossil groups (Ragagnin et al. 2019), as well as the gas properties in between galaxy clusters and groups (Biffi et al. 2022; Angelinelli et al. 2023). On larger scales, the *Magneticum* simulations demonstrated to reproduce the observed Sunyaev–Zeldovich (SZ) power spectrum (Dolag, Komatsu & Sunyaev 2016) as well as the observed thermal history of the Universe (Young, Komatsu & Dolag 2021; Chen et al. 2024). Most importantly for this work, the *Magneticum* simulations reproduce the observed level of entropy of the gas at group scales much better than other, current, cosmological hydrodynamical simulations, indicating that the model injects a realistic amount of feedback energy also at group scales (Bahar et al. 2024). Furthermore, the simulations reproduce X-ray scaling relations for galaxy groups as observed by *eROSITA*, where the central entropy of the gas as regulated by the AGN feedback plays a key in the detectability of the groups based on their X-ray luminosity (Marini et al. 2024).

To find a counterpart to the Physalis system within *Box2b/hr*, we match pairs of galaxies in the simulation based on the observational properties. After identifying such systems we can study their formation history and derive hints on possible formation scenarios as well as estimating the occurrence rate of ORCs resulting from outward moving merger shocks. The main selection criteria from the observation was the close proximity of the two galaxies, their stellar mass, as well as the remaining of some gas centred around the smaller of the two galaxies. Given the close distance of the two galaxies and their stellar masses, the dark matter haloes of the two galaxies, being typically ≈10 times more extended than the stellar body, will be already identified as one, large-scale overdense region. Assuming virial masses ($M_{\rm vir}$) in the range 1–3 × 10^{13} M$_\odot$, we found a starting set of ∼26 000 low-mass groups within the volume of the simulation (e.g. 0.75 Gpc^3). We then applied the following, additional requirements: (a) the system contains two massive galaxies, where the second most massive has at least 1/3 of the total stellar mass; (b) the 3D distance between the two massive galaxies is less than 70 kpc; (c) the galaxies' stellar masses within a 20 kpc aperture differ by more than 10 per cent; (d) at least one galaxy has a total gas mass greater than 10^{10} M$_\odot$ within the 20 kpc aperture; (e) the smaller galaxy (in terms of stellar mass) has at least 10 per cent more hot gas ($T > 10^6$ K) than the larger galaxy within the 20 kpc aperture. These additional requirements left us with only 10 haloes within the simulation volume.

Forcing the galaxies not to be star forming and not showing obvious tidal features, we are left with only one candidate system, for which we studied the evolution in detail. This already demonstrates that such merger configurations are quite rare, being consistent with the low number of observed ORCs. A visual impression of its evolution is shown in Fig. 7. The detailed investigation of the evolution of this peculiar system showed several interesting details. On the one hand, the group was generally X-ray bright before the first passage of the two galaxies. However, during this first passage, cold gas is channelled onto the BH of the more massive galaxy that sits closer to the centre of the total potential and the common gas envelope is energized and expanded so that it is below the direct detection threshold of our current *XMM* observations. A remaining fraction of concentrated, hot gas is still bound to the local potential of the smaller, satellite galaxy and matches in its properties the observations. Interestingly, the BH in the more massive galaxy grows by ∼10^8 M$_\odot$ during the first passage, corresponding to an energy release of ∼10^{59} erg, which matches the energy content inside the radio-emitting region of the ORC inferred by the X-ray observations. Fig. 8 shows the mock observations of the simulated system at the time when it was selected in the simulation, where the synthetic SZ map also shows the distribution of the pressure within the system. This broadly confirms the picture that such ORCs/radio shells could be produced by a combination of energy release from the AGN and subsequent lightening up in radio by merger shocks travelling through the CGM of these systems.

In Fig. 6, we highlight the location of the Physalis system (red squares) and other ORCs in the radio power versus mass diagram typically used to explore cluster scaling relations. As more ORCs are discovered and used to populate this diagram, we can explore their similarity to cluster relics. While the latter have additional physical processes, which makes the relation steeper, ORCs could indicate that they are as efficient in converting the merger energy into radio power than the most efficient clusters, or even more (in the case of the Cloverleaf), indicating that energization by the AGN seems to be a quite efficient process.

5 CONCLUSIONS

The ASKAP discovery of the ORC-like Physalis system together with the *XMM–Newton* detection of diffuse X-ray emission is a great opportunity to investigate and understand the formation mechanism of such large-scale radio shells around such a nearby, interacting galaxy pair. While the shells are centred on the brightest and most massive group galaxy, ESO 184-G042, the hot gas is found offset by 30 kpc in and around the less massive companion galaxy, LEDA 418116 (see Fig. 2). Such offset between the central radio emission and the hot gas, also just recently seen in the Cloverleaf system (Bulbul et al. 2024), is likely a signature of the unsettled state of the system, similarly to what is sometimes observed in clusters (e.g. Rosignoli et al. 2024). The orientation of the radio shells (perpendicular to the linearly aligned group galaxies) together with the extended envelope of intragroup light surrounding the central galaxy pair, and the offset hot gas, suggests that a full merger is in progress. We suggest that the Physalis radio shells are formed by

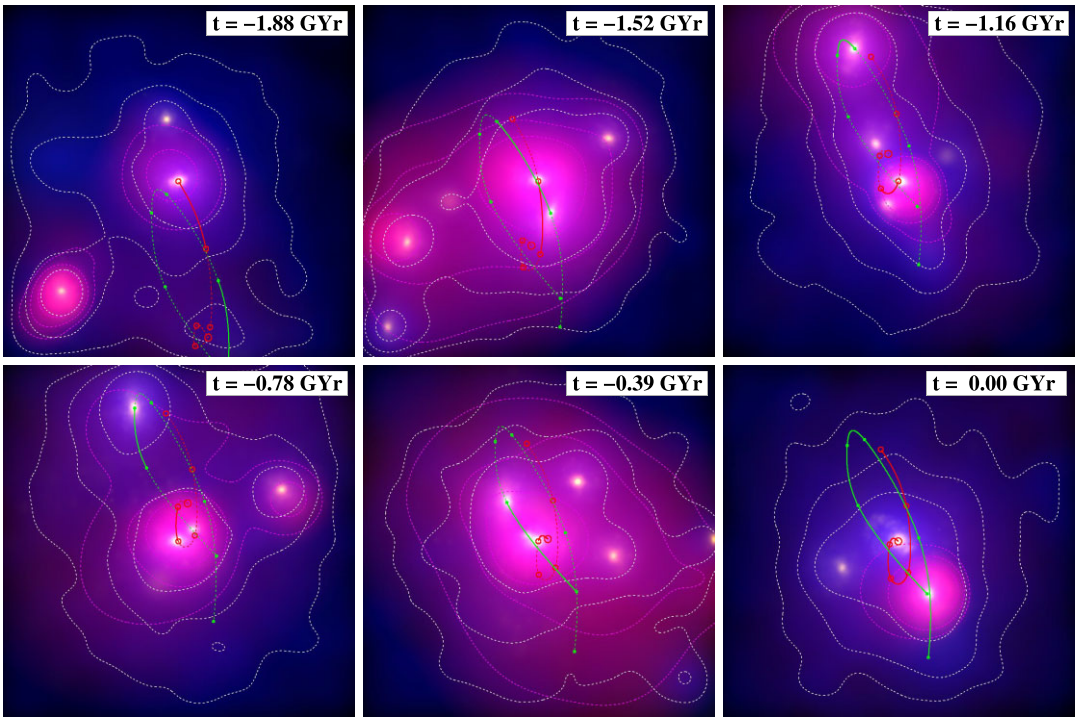

Figure 7. Evolution (from top left to bottom right) of the candidate system selected from the *Magneticum Box2b/hr* simulation of the last ∼2 Gyr. Shown is a 200 kpc comoving region centred on the most massive galaxy of the group. The background composite image reflects the dark matter (blue channel), the X-ray emission (red channel), and the SDSS K-band luminosity of the stellar component (white). To better show the assembly of the group, the white contours are drawn from the dark matter distribution, indicating that very early on the common dark matter halo is in place. In contrast, the common X-ray atmosphere [intergalactic medium (IGM), indicated as pink contours] only builds up gradually reaching the most similar shape compared to the dark matter roughly 500 Myr before the final time at which the group was selected as counterpart. The circles along the trajectories of the two main galaxies are indicating the size of the BHs in the centres of the galaxies. The BH in the most massive galaxy grows significantly between the last times shown, releasing a large amount of energy in the form of feedback, which energizes and lifts a large fraction of the IGM to larger distances, so that only the part associated with the second galaxy stays visible.

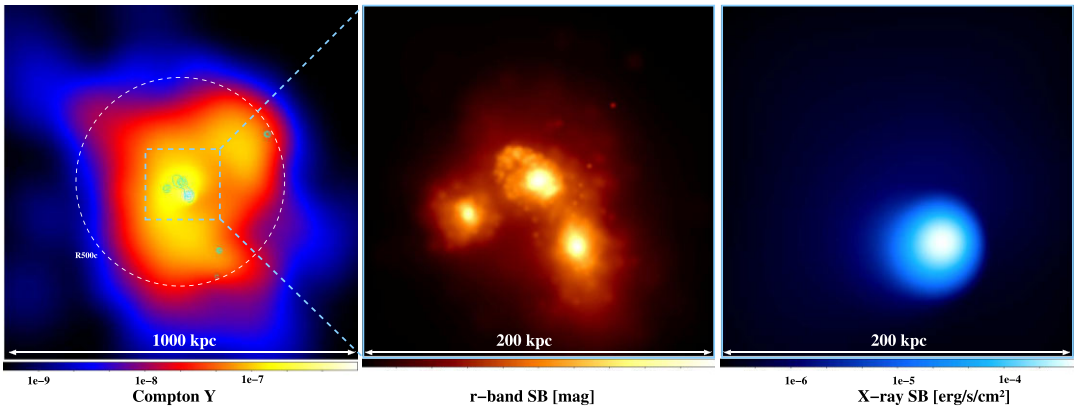

Figure 8. Mock images from the simulated counterpart of the Physalis system. Left: The large-scale thermal SZ signal, highlighting the pressure distribution within the halo and the impact of the AGN feedback. Overlaid in cyan are the contours from the SDSS r-band mocks, indicating the positions of the central galaxies. The white, dashed circle indicates the halo radius of R_{500c}. Middle: The optical SDSS r-band mocks in the central 200 kpc region. Right: The X-ray surface brightness in the same region based on the emission in the 0.1–2.4 keV band, highlighting the offset between the X-ray emission peak, which is centred on the companion galaxy, and the central galaxy.

outward moving merging shocks (Dolag et al. 2023b), and while resembling cluster radio relics (see also Koribalski et al. 2024), they are smaller and associated with mergers in galaxy groups. An investigation of the radio power to mass relation is underway. This is the first time that radio relics around galaxy groups have been detected.

In the Physalis system, the derived temperature and density of the hot X-ray emitting gas combined with the ASKAP flux densities

allow us to place constraints on the energetics of the event that led to the ORC/radio shell formation and differentiate between possible scenarios. The required release of 10^{59} erg over a period of a few hundred million years might be provided by an episode of SMBH activity triggered by gas inflows during the merger of two central galaxies accompanying the build-up of a compact group. Strong shocks are needed to accelerate electrons from the thermal pool, but even weak shocks may be able to reaccelerate fossil electrons. We were able to identify and explore one matching galaxy system in the *Magneticum* simulations and present snapshots of its evolution, underlining the rarity of such energetic events. This is an exciting field that is growing rapidly as more ORCs and radio shell systems are being discovered.

ACKNOWLEDGEMENTS

We thank the referee for insightful comments that helped us to improve the paper. We also thank Norbert Schartel for his support of the *XMM–Newton* DDT observations. IK and KD were supported by the Excellence Cluster ORIGINS that is funded by the Deutsche Forschungsgemeinschaft (DFG, German Research Foundation) under Germany's Excellence Strategy – EXC-2094-390783311 – and the COMPLEX project from the European Research Council (ERC) under the European Union's Horizon 2020 Framework Programme grant agreement ERC-2019-AdG 882679.

The ASKAP is part of the Australia Telescope National Facility (ATNF) that is managed by CSIRO. Operation of ASKAP is funded by the Australian Government with support from the National Collaborative Research Infrastructure Strategy. ASKAP uses the resources of the Pawsey Supercomputing Centre. Establishment of ASKAP, the Murchison Radio-astronomy Observatory (MRO), and the Pawsey Supercomputing Centre are initiatives of the Australian Government, with support from the Government of Western Australia and the Science and Industry Endowment Fund. This paper includes archived data obtained through the CSIRO ASKAP Science Data Archive (CASDA). We acknowledge the Wajarri Yamatji as the traditional owners of the Observatory site.

This project used public archival data from the Dark Energy Survey (DES). Funding for the DES Projects has been provided by the U.S. Department of Energy, the U.S. National Science Foundation, the Ministry of Science and Education of Spain, the Science and Technology Facilities Council of the United Kingdom, the Higher Education Funding Council for England, the National Center for Supercomputing Applications at the University of Illinois at Urbana–Champaign, the Kavli Institute of Cosmological Physics at the University of Chicago, the Center for Cosmology and Astro-Particle Physics at the Ohio State University, the Mitchell Institute for Fundamental Physics and Astronomy at Texas A&M University, Financiadora de Estudos e Projetos, Fundação Carlos Chagas Filho de Amparo à Pesquisa do Estado do Rio de Janeiro, Conselho Nacional de Desenvolvimento Científico e Tecnológico and the Ministério da Ciência, Tecnologia e Inovação, the Deutsche Forschungsgemeinschaft, and the Collaborating Institutions in the DES.

DATA AVAILABILITY

The ASKAP data products are publicly available in the CSIRO ASKAP Science Data Archive (CASDA) at data.csiro.au/domain/casdaObservation. The *XMM–Newton* data are available at www.cosmos.esa.int/web/xmm-newton/too-details.

Additional data processing and analysis was conducted using the MIRIAD software[5] and the KARMA visualization[6] packages.

REFERENCES

Abbott R. et al., 2020, Phys. Rev. D, 102, 043015
Angelinelli M., Ettori S., Dolag K., Vazza F., Ragagnin A., 2023, A&A, 675, A188
Antonini F., Gieles M., 2020, Phys. Rev. D, 102, 123016
Antonini F., Gieles M., Dosopoulou F., Chattopadhyay D., 2023, MNRAS, 522, 466
Appleton P. N. et al., 2023, ApJ, 951, 104
Arnaud K. A., 1996, in Jacoby G. H., Barnes J., eds, ASP Conf. Ser. Vol. 101, Astronomical Data Analysis Software and Systems V. Astron. Soc. Pac., San Francisco, p. 17
Bahar Y. E. et al., 2024, preprint (arXiv:2401.17276)
Beck R., Krause M., 2005, Astron. Nachr., 326, 414
Beck A. M. et al., 2016, MNRAS, 455, 2110
Biffi V., Dolag K., Böhringer H., 2013, MNRAS, 428, 1395
Biffi V., Mernier F., Medvedev P., 2018a, Space Sci. Rev., 214, 123
Biffi V., Dolag K., Merloni A., 2018b, MNRAS, 481, 2213
Biffi V., Dolag K., Reiprich T. H., Veronica A., Ramos-Ceja M. E., Bulbul E., Ota N., Ghirardini V., 2022, A&A, 661, A17
Bryan G. L., Norman M. L., 1998, ApJ, 495, 80
Bulbul E. et al., 2024, A&A, 685, L2
Chen Z. et al., 2024, Phys. Rev. D, 109, 063513
Churazov E., Forman W., Jones C., Böhringer H., 2003, ApJ, 590, 225
Coil A. L. et al., 2024, Nature, 625, 459
de Gasperin F., van Weeren R. J., Brüggen M., Vazza F., Bonafede A., Intema H. T., 2014, MNRAS, 444, 3130
Dehnen W., Aly H., 2012, MNRAS, 425, 1068
de Vaucouleurs G., de Vaucouleurs A., Corwin H. G., Jr, Buta R. J., Paturel G., Fouque P., 1991, Third Reference Catalogue of Bright Galaxies. Vol. I: Explanations and References. Vol. II: Data for Galaxies Between 0^h and 12^h. Vol. III: Data for Galaxies Between 12^h and 24^h. Springer, New York
Dey A. et al., 2019, AJ, 157, 168
Díaz-Giménez E., Mamon G. A., Pacheco M., Mendes de Oliveira C., Alonso M. V., 2012, MNRAS, 426, 296
Dolag K., Jubelgas M., Springel V., Borgani S., Rasia E., 2004, ApJ, 606, L97
Dolag K., Vazza F., Brunetti G., Tormen G., 2005, MNRAS, 364, 753
Dolag K., Borgani S., Murante G., Springel V., 2009, MNRAS, 399, 497
Dolag K., Komatsu E., Sunyaev R., 2016, MNRAS, 463, 1797
Dolag K., Mevius E., Remus R.-S., 2017, Galaxies, 5, 35
Dolag K. et al., 2023a, Am. Astron. Soc. High Energy Astrophys. Division Meeting, #20, 110.12
Dolag K., Böss L. M., Koribalski B. S., Steinwandel U. P., Valentini M., 2023b, ApJ, 945, 74
Duchesne S. W. et al., 2024, Publ. Astron. Soc. Aust., 41, e026
Eke V. R., Cole S., Frenk C. S., 1996, MNRAS, 282, 263
Evrard A. E. et al., 2008, ApJ, 672, 122
Fabjan D., Borgani S., Tornatore L., Saro A., Murante G., Dolag K., 2010, MNRAS, 401, 1670
Ferragamo A. et al., 2021, A&A, 655, A115
Forbes D. A., 2017, MNRAS, 472, L104
Geng A., Beck A. M., Dolag K., Bürzle F., Beck M. C., Kotarba H., Nielaba P., 2012, MNRAS, 426, 3160
Girelli G., Pozzetti L., Bolzonella M., Giocoli C., Marulli F., Baldi M., 2020, A&A, 634, A135
Gu L. et al., 2019, Nat. Astron., 3, 838
Gupta N., Saro A., Mohr J. J., Dolag K., Liu J., 2017, MNRAS, 469, 3069
Gupta N., Huynh M., Norris R. P., Wang X. R., Hopkins A. M., Andernach H., Koribalski B. S., Galvin T. J., 2022, Publ. Astron. Soc. Aust., 39, e051

[5]https://www.atnf.csiro.au/computing/software/miriad/
[6]https://www.atnf.csiro.au/computing/software/karma/

Hirschmann M., Dolag K., Saro A., Bachmann L., Borgani S., Burkert A., 2014, MNRAS, 442, 2304
Hotan A. W. et al., 2021, Publ. Astron. Soc. Aust., 38, e009
Hurley-Walker N. et al., 2017, MNRAS, 464, 1146
Hurley-Walker N. et al., 2022, Publ. Astron. Soc. Aust., 39, e035
Jansen F. et al., 2001, A&A, 365, L1
Johnston S. et al., 2008, Exp. Astron., 22, 151
Jones D. H. et al., 2009, MNRAS, 399, 683
Jones A. et al., 2023, A&A, 680, A31
Karademir G. S., Remus R.-S., Burkert A., Dolag K., Hoffmann T. L., Moster B. P., Steinwandel U. P., Zhang J., 2019, MNRAS, 487, 318
Komatsu E. et al., 2011, ApJS, 192, 18
Koribalski B. S., 2012, Publ. Astron. Soc. Aust., 29, 359
Koribalski B. S., 2022, "The technological and scientific development of ASKAP," 2022 3rd URSI Atlantic and Asia Pacific Radio Science Meeting (AT-AP-RASC), Gran Canaria, Spain, 2022, pp. 1-4, (arXiv:2208.08245)
Koribalski B. S. et al., 2004, AJ, 128, 16
Koribalski B. S. et al., 2020, Ap&SS, 365, 118
Koribalski B. S., Norris R. P., Andernach H., Rudnick L., Shabala S., Filipović M., Lenc E., 2021, MNRAS, 505, L11
Koribalski B. S. et al., 2024, MNRAS, 531, 3357
Kraft R. P. et al., 2012, ApJ, 749, 19
Kraft R. et al., 2022, preprint (arXiv:2211.09827)
Kumari S., Pal S., 2024a, MNRAS, 527, 11233
Kumari S., Pal S., 2024b, A&A, 683, A175
Lansbury G. B., Jarvis M. E., Harrison C. M., Alexander D. M., Del Moro A., Edge A. C., Mullaney J. R., Thomson A. P., 2018, ApJ, 856, L1
Lauberts A., Valentijn E. A., 1989, The Surface Photometry Catalogue of the ESO-Uppsala Galaxies. European Southern Observatory, Garching
Lin Y.-H., Yang H.-Y. K., 2024, preprint (arXiv:2401.08207)
Lochner M., Rudnick L., Heywood I., Knowles K., Shabala S. S., 2023, MNRAS, 520, 1439
Lotz M., Remus R.-S., Dolag K., Biviano A., Burkert A., 2019, MNRAS, 488, 5370
Lovisari L., Ettori S., Gaspari M., Giles P. A., 2021, Universe, 7, 139
Lustig P. et al., 2023, MNRAS, 518, 5953
Makarov D., Prugniel P., Terekhova N., Courtois H., Vauglin I., 2014, A&A, 570, A13
Malin D. F., Carter D., 1980, Nature, 285, 643
Malin D. F., Carter D., 1983, ApJ, 274, 534
Marini I. et al., 2024, preprint (arXiv:2404.12719)
Markevitch M., Gonzalez A. H., David L., Vikhlinin A., Murray S., Forman W., Jones C., Tucker W., 2002, ApJ, 567, L27
Mauch T., Murphy T., Buttery H. J., Curran J., Hunstead R. W., Piestrzynski B., Robertson J. G., Sadler E. M., 2003, MNRAS, 342, 1117
Montes M., 2022, Nat. Astron., 6, 308
Naab T., Ostriker J. P., 2017, ARA&A, 55, 59
Nolting C., Ball J., Nguyen T. M., 2023, ApJ, 948, 25
Norris R. P. et al., 2011, Publ. Astron. Soc. Aust., 28, 215
Norris R. P. et al., 2021a, Publ. Astron. Soc. Aust., 38, e003
Norris R. P. et al., 2021b, Publ. Astron. Soc. Aust., 38, e046
Norris R. P. et al., 2022, MNRAS, 513, 1300
Pasini T. et al., 2022, A&A, 661, A13
Ragagnin A., Dolag K., Moscardini L., Biviano A., D'Onofrio M., 2019, MNRAS, 486, 4001
Ragagnin A., Saro A., Singh P., Dolag K., 2021, MNRAS, 500, 5056
Randall S. W., Jones C., Kraft R., Forman W. R., O'Sullivan E., 2009, ApJ, 696, 1431
Rawes J., Birkinshaw M., Worrall D. M., 2018, MNRAS, 480, 3644
Ridley E. J. et al., 2024, MNRAS, 531, 1905
Rong Y., Shen J., Hua Z., 2024, MNRAS, 531, L9
Rosignoli L. et al., 2024, ApJ, 963, 8
Rupke D. S. N., Coil A. L., Whalen K. E., Moustakas J., Tremonti C. A., Perrotta S., 2024, ApJ, 967, 51
Shabala S. S. et al., 2024, Publ. Astron. Soc. Aust., 41, e024
Skrutskie M. F. et al., 2006, AJ, 131, 1163
Smith R. K., Brickhouse N. S., Liedahl D. A., Raymond J. C., 2001, ApJ, 556, L91
Spavone M. et al., 2018, ApJ, 864, 149
Springel V., Hernquist L., 2002, MNRAS, 333, 649
Springel V., White S. D. M., Tormen G., Kauffmann G., 2001, MNRAS, 328, 726
Springel V., Di Matteo T., Hernquist L., 2005, MNRAS, 361, 776
Steinborn L. K., Dolag K., Comerford J. M., Hirschmann M., Remus R.-S., Teklu A. F., 2016, MNRAS, 458, 1013
Tempel E., Kruuse M., Kipper R., Tuvikene T., Sorce J. G., Stoica R. S., 2018, A&A, 618, A81
Tornatore L., Borgani S., Springel V., Matteucci F., Menci N., Murante G., 2003, MNRAS, 342, 1025
Tornatore L., Borgani S., Dolag K., Matteucci F., 2007, MNRAS, 382, 1050
van Weeren R. J., de Gasperin F., Akamatsu H., Brüggen M., Feretti L., Kang H., Stroe A., Zandanel F., 2019, Space Sci. Rev., 215, 16
Velović V., Cotton W. D., Filipović M. D., Norris R. P., Barnes L. A., Condon J. J., 2023, MNRAS, 523, 1933
Wegner G. et al., 2003, AJ, 126, 2268
Wen Z. L., Han J. L., 2024, ApJS, 272, 39
Wiersma R. P. C., Schaye J., Theuns T., Dalla Vecchia C., Tornatore L., 2009, MNRAS, 399, 574
Yamasaki S., Sarkar K. C., Li Z., 2024, MNRAS, 528, 3854
Yang S. et al., 2019, ApJ, 875, 59
Young S., Komatsu E., Dolag K., 2021, Phys. Rev. D, 104, 083538
Zhang C., Churazov E., Forman W. R., Lyskova N., 2019, MNRAS, 488, 5259
Zou H., Gao J., Zhou X., Kong X., 2019, ApJS, 242, 8

This paper has been typeset from a TEX/LATEX file prepared by the author.